ADABOOST-BASED DETECTION AND SEGMENTATION OF BIORESORBABLE VASCULAR SCAFFOLDS STRUTS IN IVOCT IMAGES

Yifeng Lu[⋆†] *Yihui Cao*[⋆‡†] *Qinhua Jin*[*] *Yundai Chen*[*] *Qinye Yin*[‡] *Jianan Li*[⋆] *Rui Zhu*[⋆] *Wei Zhao*[⋆]

[⋆] State Key Laboratory of Transient Optics and Photonics, Xi'an Institute of Optics and Precision Mechanics, Chinese Academy of Sciences, Xi'an, P. R. China
[†] University of Chinese Academy of Sciences, Beijing, P. R. China
[‡] School of the Electronic and Information Engineering, Xi'an Jiaotong University, Xi'an, P. R. China
[*] Department of Cardiology, Chinese PLA General Hospital, Beijing, P. R. China

ABSTRACT

Bioresorbable Vascular Scaffolds (BVS) are the most promising type of stent in percutaneous coronary intervention. For accurate BVS struts apposition assessment, intravascular optical coherence tomography (IVOCT) is the state-of-the-art imaging modality. However, manual analysis for IVOCT frames is time consuming and labor intensive. In this paper, we propose an automatic method for BVS struts center and region detection based on Adaboost algorithm and Haar-like features. Then, dynamic programming algorithm is applied to segment the contour of BVS struts. Based on the segmentation results, the apposed or malapposed struts can be automatically distinguished. By comparing the manual and automatic detection and segmentation results, our method correctly detected and segmented 87.7% of 4029 BVS struts with 18.6% false positives. The average Dice's coefficient for the correctly detected struts was 0.78. In conclusion, the evaluation suggested that this method is accurate and robust for BVS struts detection and segmentation.

Index Terms— BVS detection and segmentation, Adaboost, Haar-like features, IVOCT

1. INTRODUCTION

Bioresorbable vascular scaffolds (BVS) have shown a promising improvement to metallic stents in percutaneous coronary intervention [1]. However, in clinical BVS stenting application, malapposition may happen and may lead to adverse cardiovascular events such as late stent thrombosis and myocardial infarction. Therefore, it is vital to detect malapposition immediately after stenting. Intravascular optical coherence tomography (IVOCT), providing with superior resolution, is currently the state-of-the-art imaging modality which enables malapposition detection [2]. Frames after BVS stenting are shown in Fig. 1, where BVS struts are represented by bright rectangular boundaries with box-shape black cores inside. If a strut is distant from lumen contour, it is defined as a malapposed strut. Otherwise it is an apposed strut.

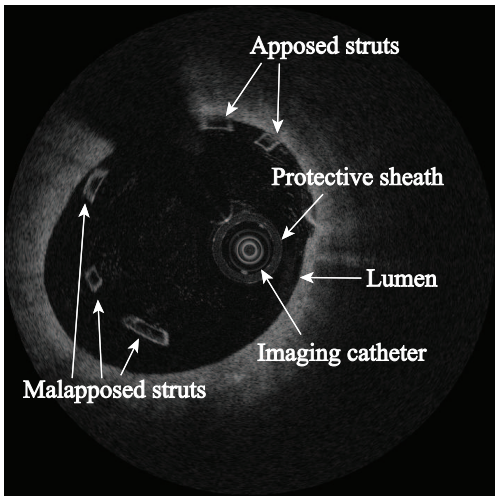

Fig. 1. An IVOCT image after BVS stenting. Apposed struts, malapposed struts, imaging catheter, protective sheath and lumen are shown respectively.

In current practice, malapposition analysis for IVOCT images is mainly conducted manually. However, quantitative BVS evaluation requires accurate marking and measurement of all struts in a pullback run. It is thus time consuming and labor intensive. From that an automatic method for BVS struts detection and malapposition analysis is highly desired.

Previously, few articles about automatic BVS analysis in IVOCT images have been published. To the best of our knowledge, the only work that has been published is conducted by Wang et al. [3], whose method is based on gray and gradient feature and uses a fixed threshold for struts detection and segmentation. However, this method may have some problems with generalization since the threshold is fixed.

To obtain better generalization, in this paper, machine

This work is supported by the Chinese Academy of Science and technology service network plan (Grant No. KFJ-SW-STS-185).

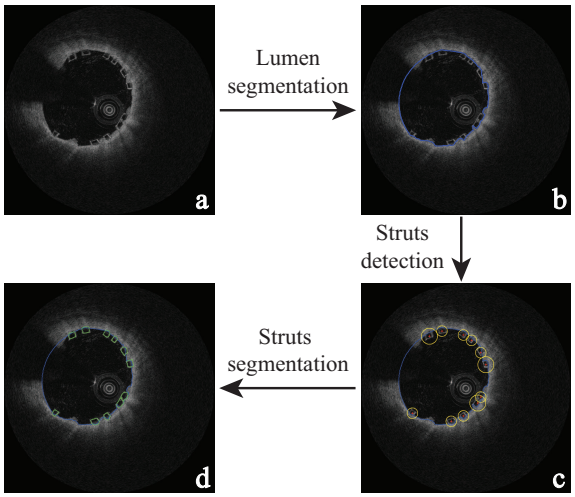

Fig. 2. Procedures of BVS struts detection.

learning is applied to train a cascade of Adaboost classifiers based on Haar-like features for BVS struts detection. Besides, dynamic programming (DP) [4] is applied to segment the struts after detecting the struts center position and region. Based on above detection and segmentation, IVOCT images can be analyzed automatically for malapposition detection. With three aspects mentioned above, our method enables automatic BVS struts analysis. To evaluate the method, we compared the manual and automatic detection results. Qualitative and quantitative validation illustrated that the presented method is effective and robust.

2. METHOD

As is shown in Fig. 2, the pipeline of our method mainly contains three steps: 1) Lumen segmentation; 2) Struts detection; 3) Struts segmentation. In the following subsections, each step is described in more detail.

2.1. Lumen segmentation

In order to obtain better analysis for struts malapposition, lumen segmentation is needed. Many researchers have previously proposed lumen segmentation methods [5–8], among which the classic Dynamic Programming (DP) algorithm has proven to be highly robust and efficient. Therefore, in this paper, we utilize DP optimization method proposed by Wang et al. [7] to find and visualize lumen boundary. The main strategy is to transform the IVOCT images into polar coordinate system and search for a path throughout the polar image with the optimal cost. The path is then transformed back into the Cartesian coordinate system and the corresponding detected lumen is represented by this path. Fig. 2(b) shows an example of lumen segmentation in an IVOCT image where lumen contour is represented by blue curves.

Fig. 3. The basic Haar-like features selected for Adaboost training.

2.2. Struts detection

Ever since the publication of the work of Viola et al. [9], the field of object detection has developed fast. Haar-like features, as proposed in Viola's work, are quite effective for line, edge and diagonal detection and are thus successfully applied to face detection. BVS struts, with rectangular bright boundaries around and box-shape black cores inside as Fig. 1 shows, share similar features with facial structures and could potentially be detected by Haar-like features in a similar way as face detection. Therefore, in our method, a set of basic Haar-like features is selected for BVS struts detection. However, given the large number of Haar-like features within a sub-image, it is vital to find an efficient method for feature selection. Due to the advantage of high accuracy and little possibility of over-fitting, Adaboost algorithm has proven to be quite effective and robust for feature selection. Therefore, in our method, a cascade of Adaboost-based classifiers, combined with a set of Haar-like features, is selected for the BVS struts detection. Our goal is to find a seed point representing the center position of a detected strut and determine a region that completely contains the strut. Our approach for struts detection mainly consists of two parts: training and testing.

In the training part, there are three main steps: 1) Selecting training samples. As Fig. 5 shows, samples are labeled by an expert from IVOCT images of different patients and are gathered for training. Positive samples should include only one complete BVS strut per sub-image and negative samples are acquired randomly from non-strut regions. The samples are then normalized to a common size $N \times N$ pixels; 2) Extracting Haar-like features. Fig. 3 visualizes the set of basic feature types selected for Adaboost training. These Haar-like features are quite effective for line, edge and diagonal detection, and are capable of detecting BVS struts with few false positives. The basic Haar-like features are calculated at different positions and scales within each sample image to form a data matrix; 3) Training classifiers using Adaboost. Based on the above matrix, a cascade of classifiers is trained using Adaboost to select the most distinguishable Haar-like features and compute the corresponding thresholds and weights.

In the testing part, a sliding window of size $N \times N$ moves at a step of T pixels throughout the IVOCT image at different scales S to compute the score of each sub-image based on the previously selected Haar-like features. If the score calculated by each strong classifier is larger than the corresponding threshold, the sub-image is counted as a candidate. The position of the detected strut is represented by the center point of this sub-image, namely the seed point.

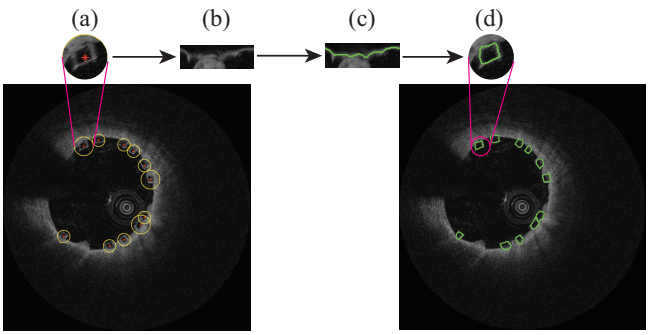

Fig. 4. Strut segmentation process. Each strut is transformed into polar coordinate system and a path is found with the optimal cost. The path is then transformed back into Cartesian coordinate system to represent the segmented strut.

In addition, since struts size varies within each IVOCT image, it is vital to determine a region of interest (ROI) for each detected strut to completely contain the strut. Based on the information of window scale, ROI could be represented by a circle whose radius R is defined as: $R = S \times N/2$, where S is the scale at which a strut is successfully detected and N is the initial size of the sliding window. Fig. 2(c) shows an example of BVS struts detection where red dots refer to seed points and yellow curves represent ROI.

2.3. Struts segmentation

In order to visualize the detected struts for further analysis, the struts need to be segmented. In our study, DP algorithm is adopted to segment the struts. Fig. 4 shows the main process of struts segmentation.

Firstly, based on the seed point and radius R, each detected BVS strut within ROI, as Fig. 4(a) shows, is transformed into polar coordinate system characterized by angle θ and depth d. Fig. 4(b) demonstrates the transformed image of ROI in polar coordinate system. Suppose that the size of ROI in polar coordinate system is $M \times R$. Our goal is to search for a path from column 1 to column M with the optimal cost C. Considering the connectivity between adjacent columns, this problem can be broken into some subproblems and resolved by DP algorithm. In this way, the cost C can be defined as:

$$\begin{aligned} C(\theta, d) &= E(\theta, d), && \theta = 1 \\ C(\theta, d) &= \min C(\theta - 1, d^*) + E(\theta, d), && 1 < \theta \leq M \end{aligned} \tag{1}$$

where $C(\theta, d)$ is the accumulated cost from column 1 to point (θ, d), $d^* \in [d - m, d + m]$, and m is a neighborhood coefficient. $E(\theta, d)$ is the energy function in point (θ, d) defined as:

$$E = I * w \tag{2}$$

where I is the transformed image of ROI in polar coordinate system, w is an edge filter sensitive to horizontal edges, and $*$ refers to convolution. As is shown in Fig. 4(c), the strut contour can be found by globally minimizing the accumulated cost C and back tracking the path. The image, along with the strut segmentation data, is then transformed back into Cartesian coordinate system. Fig. 4(d) shows the final segmentation result in Cartesian coordinate system.

After having obtained the strut segmentation data, we are able to analyze the struts malapposition automatically based on the lumen and struts segmentation results. If the segmented strut contour intersects the lumen contour, it is counted as an apposed strut. Otherwise, it is a malapposed strut. Different colors are used to represent apposed and malapposed struts for more advanced analysis.

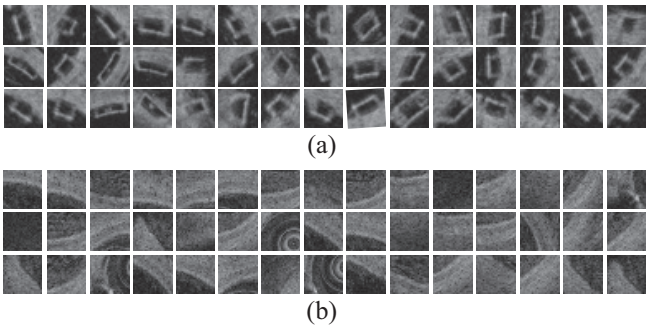

Fig. 5. Some examples of (a) positive training samples and (b) negative training samples.

3. EXPERIMENTS

3.1. Materials

In our experiment, all IVOCT images were acquired using the FD-OCT system (C7-XR system, St. Jude, St. Paul, Minnesota). The training samples were taken from 5 pullback runs of different patients at baseline. The total numbers of positive and negative samples were 1500 and 40000, respectively. Fig. 5 shows some of the positive and negative training samples selected by the expert. We finally trained a 12-stage cascaded classifier based on more than 700 Haar-like features.

In order to evaluate the performance of of our method, a total of 480 IVOCT images from another 5 different patients were taken for validation. All the BVS struts were segmented manually by an expert as the ground truth and the total number of BVS struts was 4029.

During the experiment, each parameter mentioned above was set as follows: sample image size N=24, window step T=3, window scale S={1, 1.5, 2.25, 3.375}, neighborhood coefficient m=1.

3.2. Results

Fig. 6 shows some of the detection and segmentation results using our method. The first row shows the images of ground

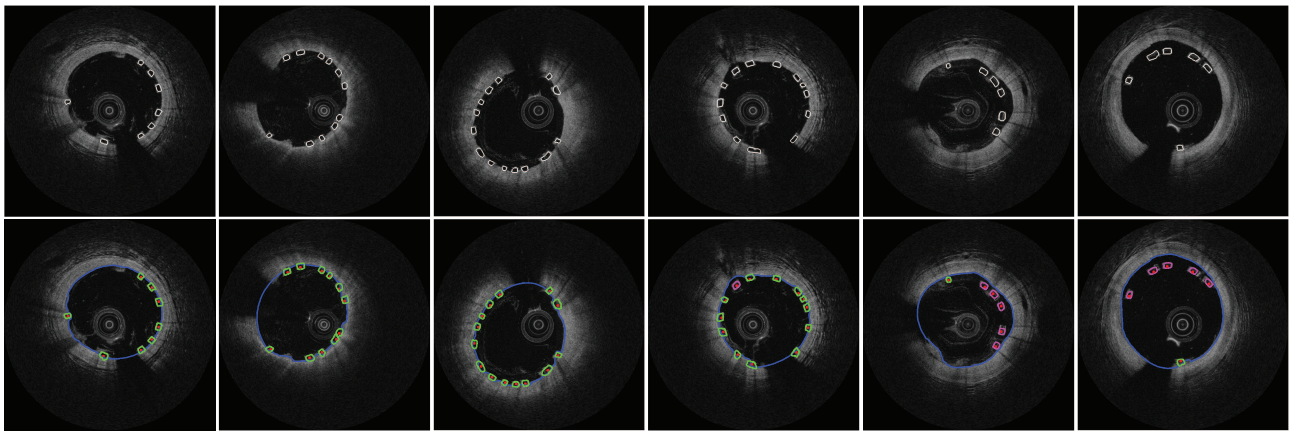

Fig. 6. The first row is the images of ground truth (white curves). The second row is the results of struts detection (red dots) and segmentation (green and purple curves are apposed and malapposed struts, respectively). Lumen contours are represented by blue curves.

Table 1. The quantitative evaluation results.

			Struts Detection				Struts Segmentation			
Data set	No.F	No.GT	TPR(%)	FPR(%)	F-measure	CPE(μm)	TPR(%)	FPR(%)	F-measure	Dice
1	81	691	94.2	14.1	0.90	28.9	93.2	15.0	0.89	0.79
2	119	928	88.8	18.3	0.85	32.4	86.3	20.6	0.83	0.79
3	86	635	83.6	18.0	0.83	28.4	82.2	19.4	0.81	0.76
4	76	603	91.9	20.5	0.85	34.4	90.0	22.1	0.84	0.79
5	118	1172	87.9	15.0	0.86	22.4	86.9	16.0	0.85	0.79
Average	-	-	89.3	17.2	0.86	29.3	87.7	18.6	0.84	0.78

No.F: Number of frames evaluated; No.GT: Number of the ground truth; TPR: True positive rate; FPR: False positive rate; CPE: Center position error.

truth represented by white curves. The second row demonstrates the result of struts detection and segmentation, where red dots mean seed points, blue curves refer to lumen contour, green curves represent apposed struts and purple curves represent malapposed struts. It can be seen that almost all BVS struts were correctly detected and segmented while few false positives occurred. Meanwhile, malapposed struts were successfully distinguished from apposed struts. Qualitative analysis suggests that our method is effective for BVS struts detection and segmentation.

Table. 1 shows the quantitative evaluation of BVS struts detection and segmentation for each pullback run. True positive rate (TPR) and false positive rate (FPR) were computed for accurate evaluation. The F-measure was also used to evaluate the performance of our classifier and was defined as: $F = 2 \times P \times R/(P + R)$, where P refers to precision and R means recall rate.

During the evaluation of struts detection, a seed point was counted as a true positive if it was completely covered by a ground truth. Otherwise, it was a false positive. On average, our method reached 89.3% TPR with 17.2% FPR, and the F-measure was 0.86. The center position error, which was defined as the distance between a correctly detected seed point and the center point of the corresponding ground truth, was calculated. In our approach, the average center position error was 29.3 μm. The evaluation of struts segmentation was based on the Dice's coefficient between the area of a segmented strut and that of a ground truth. If the Dice's coefficient is larger than 0.5, the strut was counted as a true positive. Thus, the average TPR and FPR were 87.7% and 18.6% respectively, with the F-measure at 0.84. The average Dice's coefficient for the correctly detected struts was 0.78. Quantitative evaluation shows that our method is accurate and robust.

4. CONCLUSION

In this paper, we presented an automatic method for BVS struts detection in IVOCT images based on Haar-like features and Adaboost algorithm. Then, DP algorithm was used for struts segmentation. Based on the detection and segmentation results, apposed and malapposed struts were distinguished automatically. The qualitative and quantitative evaluation shows that our method is effective and robust for BVS struts detection and segmentation, and is capable of malapposition analysis. Future work will mainly focus on sample selection and algorithm improvement to further improve the performance.

5. REFERENCES

[1] Bill D Gogas, Vasim Farooq, Yoshinobu Onuma, and Patrick W Serruys, "The absorb bioresorbable vascular scaffold: an evolution or revolution in interventional cardiology," *Hellenic J Cardiol*, vol. 53, no. 4, pp. 301–309, 2012.

[2] Hiram G Bezerra, Marco A Costa, Giulio Guagliumi, Andrew M Rollins, and Daniel I Simon, "Intracoronary optical coherence tomography: a comprehensive review: clinical and research applications," *JACC: Cardiovascular Interventions*, vol. 2, no. 11, pp. 1035–1046, 2009.

[3] Ancong Wang, Shimpei Nakatani, Jeroen Eggermont, Yoshi Onuma, Hector M Garcia-Garcia, Patrick W Serruys, Johan HC Reiber, and Jouke Dijkstra, "Automatic detection of bioresorbable vascular scaffold struts in intravascular optical coherence tomography pullback runs," *Biomedical optics express*, vol. 5, no. 10, pp. 3589–3602, 2014.

[4] Amir A Amini, Terry E Weymouth, and Ramesh C Jain, "Using dynamic programming for solving variational problems in vision," *IEEE Transactions on pattern analysis and machine intelligence*, vol. 12, no. 9, pp. 855–867, 1990.

[5] Serhan Gurmeric, Gozde Gul Isguder, Stéphane Carlier, and Gozde Unal, "A new 3-d automated computational method to evaluate in-stent neointimal hyperplasia in in-vivo intravascular optical coherence tomography pullbacks," in *International Conference on Medical Image Computing and Computer-Assisted Intervention*. Springer, 2009, pp. 776–785.

[6] Giovanni Jacopo Ughi, Tom Adriaenssens, K Onsea, Pieterjan Kayaert, C Dubois, Peter Sinnaeve, M Coosemans, Walter Desmet, and Jan Dhooge, "Automatic segmentation of in-vivo intra-coronary optical coherence tomography images to assess stent strut apposition and coverage," *The international journal of cardiovascular imaging*, vol. 28, no. 2, pp. 229–241, 2012.

[7] Zhao Wang, Hiroyuki Kyono, Hiram G Bezerra, David L Wilson, Marco A Costa, and Andrew M Rollins, "Automatic segmentation of intravascular optical coherence tomography images for facilitating quantitative diagnosis of atherosclerosis," in *SPIE BiOS*. International Society for Optics and Photonics, 2011, pp. 78890N–78890N.

[8] Stavros Tsantis, George C Kagadis, Konstantinos Katsanos, Dimitris Karnabatidis, George Bourantas, and George C Nikiforidis, "Automatic vessel lumen segmentation and stent strut detection in intravascular optical coherence tomography," *Medical physics*, vol. 39, no. 1, pp. 503–513, 2012.

[9] Paul Viola and Michael Jones, "Robust real-time object detection," *International Journal of Computer Vision*, vol. 4, no. 34–47, 2001.